MAGNETIC SUSPENSION TEST CONTROLLER FOR A NEW CONTINUOUS FLOW VENTRICULAR ASSIST DEVICE

Edgar F. Hilton,*[,1] Paul E. Allaire,* Michael J. Baloh,* Naihong Wei,* Gill Bearnson, Donald Olsen,** Pratap Khanwilkar†**

Abstract

A new continuous flow ventricular assist device using a full magnetic suspension has been constructed and tested. The magnetic suspension centers the centrifugal pump impeller within the clearance passages in the pump, thus avoiding any form of contact. The non-contact operation is designed to give very high expected mechanical reliability, large clearances, low hemolysis, and relatively small size compared to current pulsatile devices. A unique configuration of magnetic actuators on the inlet side and exit sides of the impeller give a full five axis control and suspension of the impeller. The bearing system is divided into segments which allow for three displacement axes and two angular control axes. The controller chosen for the first suspension tests consists of a decentralized set of five PID controllers. This document describes both the controller and an overview of some results pertaining to the magnetic bearing performance.

1 Introduction

This paper describes the model, a test controller, and magnetic bearing performance for the magnetic suspension of a new continuous flow ventricular assist device – henceforth referred to as *CFVAD III* – which uses a full magnetic suspension system. Said suspension system both controls five degrees of freedom and centers the impeller within the large clearance passages in the pump. Due to large clearances and the non-contact operation, both higher reliability and lower hemolysis[1] are expected as compared to existing pulsatile and rotatory devices (Allaire et al., 1996a, 1994, 1996b; Bearnson et al., 1996). The non-contact operation avoids both unwanted friction and wear and tear effects common to rolling element bearings, blood bearings, and even lubricated fluid film bearings. Thus, both the non-contact and large clearance characteristics make magnetic bearings so desirable for artificial heart applications.

CFVAD III (Figure 1) has a unique configuration of segmented magnetic actuators on both the inlet side and the exit sides (Baloh et al., 1998; Hilton, 1998). The actuator configuration provides a set of forces and moments on the impeller that center the impeller away from the walls of the pump chamber. The pump chamber itself has large clearances (above 30 mils) that reduce hemolysis and avoids thrombosis (Allaire et al., 1996a,b; Bearnson et al., 1996).

[1]Hemolysis is defined as blood cell damage associated with the crushing of blood cells. This usually leads to a condition called thrombosis, where the blood clots inside the pump, possibly leading to other medical problems.

Edgar F. Hilton's e-mail address is efhilton@alum.mit.edu, phone: (804)924-6233, fax: (804)982-2246.

*Rotating Machinery and Controls Laboratory, University of Virginia, Charlottesville, VA 22903, USA.
**Artificial Heart Laboratory, University of Utah, Salt Lake City, UT 84112, USA.
†MedQuest Products, Inc., USA.

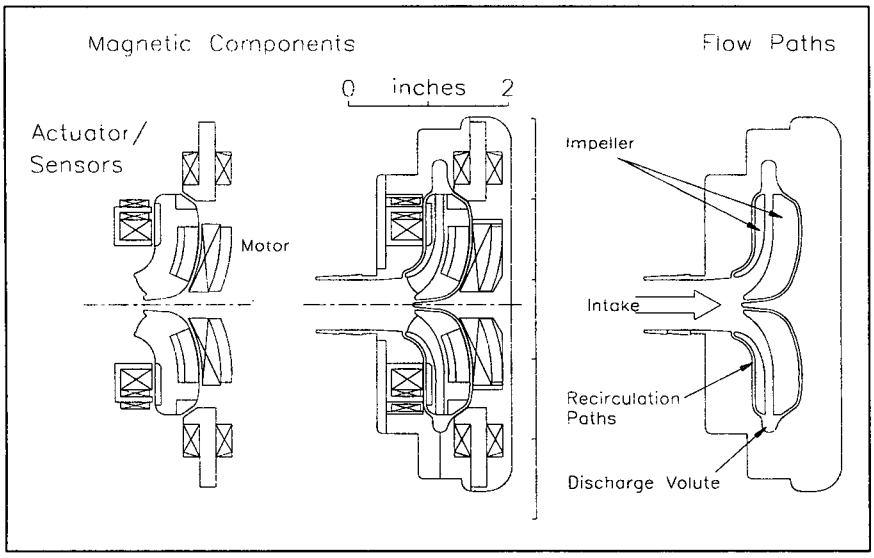

Figure 1: Detail, *CFVAD III*

A set of proportional, derivative, and integral (PID) controllers acting along the modal coordinates are used to suspend the impeller to aid in the preliminary characterization and testing of the design. Later, a multiple input/multiple output controller will be used for the final revision.

This paper does not discuss the actual design of the magnetics nor the design of the fluid chamber itself. These topics are discussed in companion papers by Baloh et al. (1998). Instead, this paper discusses the mathematical model, the controller selection, the controller design, and the controller/plant performance (Hilton, 1998).

2 The Plant

We now present the plant under consideration. The control inputs for the *CFVAD III* unit are nine currents that operate on each of the independent magnetic actuators arranged about the inlet and exit sides of the pump casing. The dynamic behavior of the impeller is measured via five outputs (Figure 2): three displacements (x, y, z) and two angular rotations (θ_x and θ_y).

The plant itself is an impeller (rotor) with forces acting along its surface (Figure 2). Sixteen points of force act along the surface of the rotor. Eight of these (henceforth referred to as the "inlet actuators" or "moment actuators") act to produce both moments about the $|x|$ and $|y|$ axes and displacement forces along the $+z$ axis. The remaining eight forces (henceforth referred to as the "radial actuators") act to primarily produce displacement forces along the $|x|$, $|y|$, and $-z$ axes, while still providing limited moments about the $|x|$ and $|y|$ axes[2].

The geometry of the inlet actuators is reminiscent of a thrust bearing segmented angularly into eight independent segments (each spanning 45°). Here, one coil (henceforth referred to as the "bias coil") wraps around inside the full thrust actuator (as is usually done for thrust actuators). In addition, each segment of the thrust actuator has its own set of windings (henceforth referred to as "moment coils"), thus allowing us to control the amount of flux passing through each segment by changing both the magnitude and polarity of each moment current[3]. In conclusion, there are a total of nine independent windings in

[2]There is a 20 degree angle between a line normal to these actuator faces and the xy plane

[3]Note that for a given bias coil current, there exists a corresponding (negative) current for each moment coil that completely nullifies the flux passing through the corresponding moment actuator.

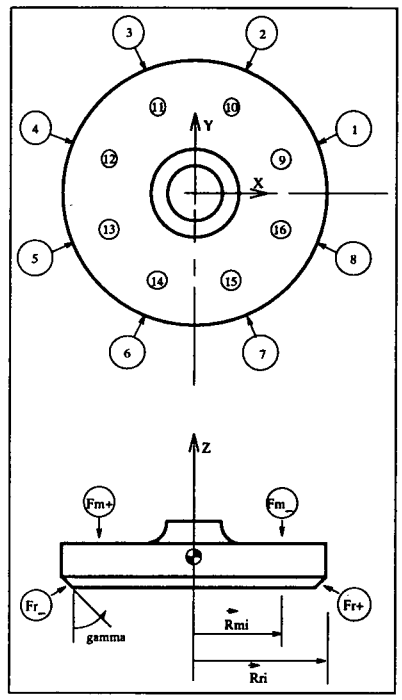

Figure 2: Force label convention and axis definition

the moment actuators.

The electrical connections for *CFVAD III* are as follows. The radial actuators are connected in pairs so that each adjacent pair of actuators behaves as an independent horseshoe electro-magnet. The inlet actuators are connected in a similar fashion, except that a fifth channel acts as a "biasing" channel (as described above). Thus, in total, the seventeen independent coils have been reduced to nine independent control channels: one bias channel (coil), four moment channels, and four radial channels.

The *linearized* forces for this magnetic bearing system are written as (Hilton, 1998)

$$\vec{F}_{magnetic} = \left\{ \begin{array}{c} \vec{F}_u \\ \vec{T}_\theta \end{array} \right\} = \mathbf{K}_I \delta\vec{I} - \mathbf{K}_X \delta\vec{U} \tag{1}$$

where $\mathbf{K}_I \in \Re^{5\times 9}$ denotes the actuator gain (the change of magnetic force due to changes in the bearing coil currents), $\mathbf{K}_X \in \Re^{5\times 5}$ (where $\mathbf{K}_X < 0$) denotes the magnetic bearing open loop stiffness (the change in the magnetic force due to changes in the position of the impeller), $\delta\vec{U} = \left[\delta x \quad \delta y \quad \delta z \quad \delta\theta_x \quad \delta\theta_y\right]^T$ denotes the generalized displacement state vector (three translational displacements and two angular displacements as described in Figure 2) and $\delta\vec{I} \in \Re^9$ denotes the input coil current vector.

The structure of the open loop stiffness matrix is

$$\mathbf{K}_X = \begin{pmatrix} \mathbf{K}_{Xuu} & \mathbf{K}_{Xu\theta} \\ \mathbf{K}_{X\theta u} & \mathbf{K}_{X\theta\theta} \end{pmatrix} = \left(\begin{array}{ccc|cc} K_{Xxx} & 0 & 0 & 0 & K_{Xx\theta_y} \\ 0 & K_{Xyy} & 0 & K_{Xy\theta_x} & 0 \\ 0 & 0 & K_{Xzz} & 0 & 0 \\ \hline 0 & K_{X\theta_x y} & 0 & K_{X\theta_x\theta_x} & 0 \\ K_{X\theta_y x} & 0 & 0 & 0 & K_{X\theta_y\theta_y} \end{array} \right) \tag{2}$$

where only the non-zero terms (as dictated by *CFVAD III* geometry) are shown for clarity, and the subscripts in $\mathbf{K}_{X\alpha\beta}$ denote the generalized state variable (α) affected by a generalized displacement (β).

For example, $\mathbf{K}_{X\theta u}$ denotes that an axial displacement (u) causes a rotation (θ). Any element in the $\mathbf{K}_{X\theta u}$ matrix would therefore specify a specific displacement or rotation. For example, $K_{Xx\theta_y}$ would imply that a rotation about the y axis will displace the rotor's center of mass along the x direction. Note that $\mathbf{K}_X$, being negative definite, destabilizes the impeller under open loop operation.

The actuator gain matrix has a similar structure:

$$\mathbf{K}_I = \begin{pmatrix} \mathbf{K}_{Iur} & \mathbf{K}_{Ium} & \mathbf{K}_{Iub} \\ \mathbf{K}_{I\theta r} & \mathbf{K}_{I\theta m} & \mathbf{K}_{I\theta b} \end{pmatrix}$$

$$= \left(\begin{array}{cccc|cccc|c} K_{Ixr_x} & 0 & K_{Ixr_{x-}} & 0 & 0 & 0 & 0 & 0 & 0 \\ 0 & K_{Iyr_y} & 0 & K_{Iyr_{y-}} & 0 & 0 & 0 & 0 & 0 \\ K_{Izr_x} & K_{Izr_y} & K_{Izr_{x-}} & K_{Izr_{y-}} & K_{Izm_x} & K_{Izm_y} & K_{Izm_{x-}} & K_{Izm_{y-}} & K_{Izb} \\ \hline 0 & K_{I\theta_x r_y} & 0 & K_{I\theta_x r_{y-}} & K_{I\theta_x m_x} & 0 & K_{I\theta_x m_{x-}} & 0 & 0 \\ K_{I\theta_y r_x} & 0 & K_{I\theta_y r_{x-}} & 0 & 0 & K_{I\theta_y m_y} & 0 & K_{I\theta_y m_{y-}} & 0 \end{array}\right) \quad (3)$$

where again, only the non-zero terms are shown for clarity. Here, the subscripts in $K_{I\alpha\gamma_*}$ denote the generalized state variable (α) affected by energizing a coil current input (γ). In this case, the input current subscript (γ) can be either a radial current ("r_*", pole faces 1-8), or a moment generating current ("m_*", pole faces 9-16), or the biasing current ("b", pole faces 9-16, in unison). The sub-subscript "*" denotes the axis most affected by energizing said current. For example, $K_{I\theta_y r_{x-}}$ implies that energizing the radial current (which normally tends to move the rotor in the negative x direction) will also produce a moment about the y axis.

Using Hamilton's Law, we construct the equations of motion

$$\begin{pmatrix} \mathbf{m} & 0 \\ 0 & \mathbf{J} \end{pmatrix} \delta\ddot{\vec{U}} = \vec{F}_{magnetic} + \vec{F}_g = \mathbf{K}_I \delta\vec{I} - \mathbf{K}_X \delta\vec{U} + \vec{F}_g \quad (4)$$

where $\mathbf{m} \in \Re^{3\times3}$ denotes the mass matrix (diagonal), $\mathbf{J} \in \Re^{2\times2}$ denotes the moment of inertia tensor, and $\vec{F}_g \in \Re^5$ denotes the disturbance input vector. Rewriting, we get

$$\mathbf{M}\delta\ddot{\vec{U}} + \mathbf{K}_X \delta\vec{U} = \mathbf{K}_I \delta\vec{I} + \vec{F}_g \quad (5)$$

where we assume that the impeller gyroscopics enter as disturbances through the $\vec{F}_g$ vector.

3 Controller Theory

We now find a stabilizing controller for the plant represented by (5). To do so, we reduce the plant to a set of five independent single input/single output systems – each existing along the natural body coordinates of *CFVAD III*. Doing so will reduce both computational overhead and controller complexity. For this application, we choose to use five independent PID (proportional, integral, and derivative) controllers whose individual transfer functions are of the form (Ogata, 1990)

$$G(s) = K_p + K_d s + \frac{K_I}{s} \quad (6)$$

The following subsections will discuss both the decomposition process and the method used to find a stabilizing controller.

3.1 Modal Decomposition

Careful analysis of Figure 2 and Equations 2 and 3 shows that energizing any one of the nine independent actuator sets will cause a force that will both move and rotate the impeller about all the three (xyz) axes. Thus, the magnetics have a coupling effect. Both the $\mathbf{K}_X$ and the $\mathbf{K}_I$ matrices are full rank. Consequently,

a decoupled system of equations must be found onto which a set of decentralized controllers may be applied to stabilize the plant.

Equation 5 can be mass normalized to give

$$\ddot{\delta\vec{U}} + \mathbf{M}^{-1}\mathbf{K}_X\delta\vec{U} = \mathbf{M}^{-1}\mathbf{K}_I\delta\vec{I} + \mathbf{M}^{-1}\vec{F}_g \tag{7}$$

Letting $\delta\vec{U} = Ae^{j\omega t}$ we find that $\dot{\delta\vec{U}} = j\omega\delta\vec{U}$ and $\ddot{\delta\vec{U}} = -\omega^2\delta\vec{U}$. Substituting into (7), rearranging slightly, and solving for the homogeneous case gives

$$\left(\mathbf{M}^{-1}\mathbf{K}_X - \omega^2\mathbf{I}\right)\delta\vec{U} = 0 \tag{8}$$

producing a standard eigenvalue (ω_i^2) and eigenvector ($\vec{\phi}_i$) problem.
Moreover, an eigenvector (mode shape) will be found for each eigenvalue so that

$$\mathbf{M}^{-1}\mathbf{K}_X\mathbf{\Phi} = \mathbf{\Phi}\mathbf{\Lambda} \tag{9}$$

where $\mathbf{\Phi} = \begin{pmatrix}\vec{\phi}_1 & \cdots & \vec{\phi}_5\end{pmatrix}$ is the modal matrix, and $\mathbf{\Lambda}_{ii} = -\omega_i^2$ $(\forall i = 1, \ldots, 5)$ is the eigenvalue matrix.

Letting $\delta\vec{U} = \mathbf{\Phi}\vec{q}$ (where q_i are the modal states) implies that (7) can be rewritten as

$$\mathbf{\Phi}\ddot{\vec{q}} + \mathbf{M}^{-1}\mathbf{K}_X\mathbf{\Phi}\vec{q} = \mathbf{M}^{-1}\mathbf{K}_I\delta\vec{I} + \mathbf{M}^{-1}\vec{F}_g \tag{10}$$

Premultiplying by $\mathbf{\Phi}^{-1}$ and rearranging the equations slightly, we find that

$$\ddot{\vec{q}} + \mathbf{\Phi}^{-1}\mathbf{M}^{-1}\mathbf{K}_X\mathbf{\Phi}\vec{q} = \mathbf{\Phi}^{-1}\mathbf{M}^{-1}\mathbf{K}_I\delta\vec{I} + \mathbf{\Phi}^{-1}\mathbf{M}^{-1}\vec{F}_g \tag{11}$$

$$\ddot{\vec{q}} + \mathbf{\Lambda}\vec{q} = \mathbf{B}_I\delta\vec{I} + \mathbf{B}_E\vec{F}_g \tag{12}$$

$$\ddot{\vec{q}} + \mathbf{\Lambda}\vec{q} = \vec{f}_u + \vec{f}_e \tag{13}$$

This leads to the independent (modally decoupled) equations

$$\ddot{q}_i - \omega_i^2 q_i = f_{i_u} + f_{i_e} \tag{14}$$

In conclusion, the goal of the *ith* PID controller would be to produce a control modal force, f_{i_u}, such that the associated modal state, q_i, will be driven to zero subject to the disturbance modal force f_{i_e}. The next section will describe the criteria on the PID parameters necessary to stabilize the above set of equations.

3.2 PID Parameter Stability Criteria

To pick a stabilizing value for the PID parameters K_p, K_d, and K_I (the proportional, derivative, and integral gains, respectively) we turn to the Routh Hurwitz stability criterion (Ogata, 1990). Referring to (14), the transfer function for each of the closed loop systems relating the state outputs to the disturbance force inputs, f_e, is given by

$$\frac{q}{f_e} = \frac{s}{s^3 + K_d s^2 + (-\omega^2 + K_p)s + K_I} \tag{15}$$

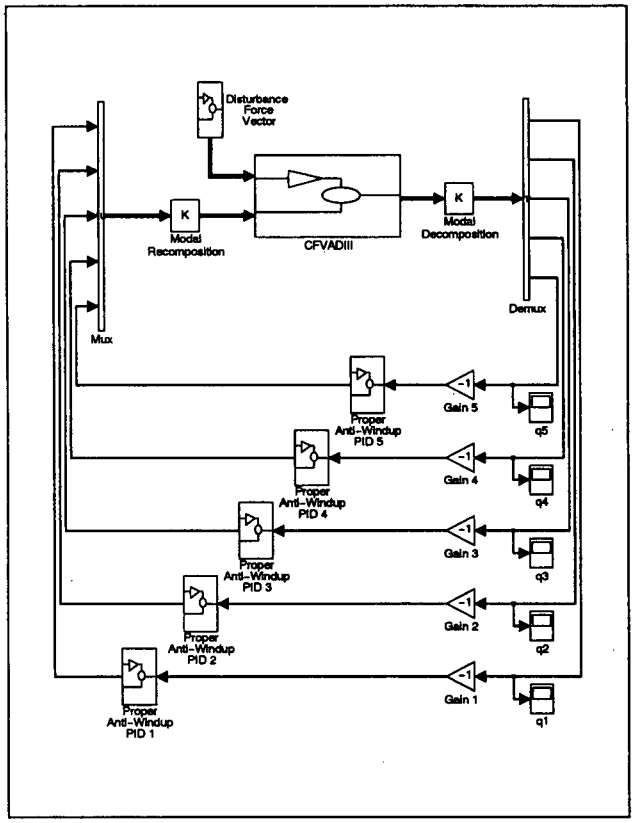

Figure 3: Overview of independent controller scheme.

Applying the Routh Hurwitz criterion, the criteria for stability of each of the modal equations are that each of the controller parameters be chosen to satisfy $K_d(-\omega^2 + K_p) - K_I > 0$ where K_p, K_I, and K_d are positive.

Note that the above relationship will merely give us a general relationship useful in finding a stabilizing controller. Each controller parameter can then be tuned according to well known controller tuning guidelines such as the Ziegler-Nichols PID tuning rules (Ogata, 1990).

3.3 Controller Overview

In Figure 3, an overview of the system is presented. The "CFVAD III" block contains the input and output characteristics of the *CFVAD III* system, where both 9 current control inputs and 5 disturbance forces and torques enter through the left center and top left, respectively; and 5 sensor (Voltage) outputs exit through the right. These sensor outputs are decomposed into modal coordinates (q_i) and fed via negative feedback to the PID controllers. Each controller then commands a modal force, f_{i_u}, which is then converted into control currents and fed to the input of the "CFVAD III" block.

Figure 4 shows the detail of the "CFVAD III" block itself. On the left, both disturbance inputs (forces and torques) and the desired control inputs (currents) enter the system. These control currents are clipped at both 5 and 0 Amperes for the radial actuators, and at both $-1.25I_{bias}$ (where I_{bias} denotes the bias coil current) and 5 Amperes for the moment actuators. Both the clipped currents and the disturbance forces and torques act directly on the plant, denoted here by an actuator gain matrix $\mathbf{K}_I$, a set of integrators, and a negative feedback loop denoting the linearized open-loop stiffness matrix $\mathbf{K}_X$. The output from

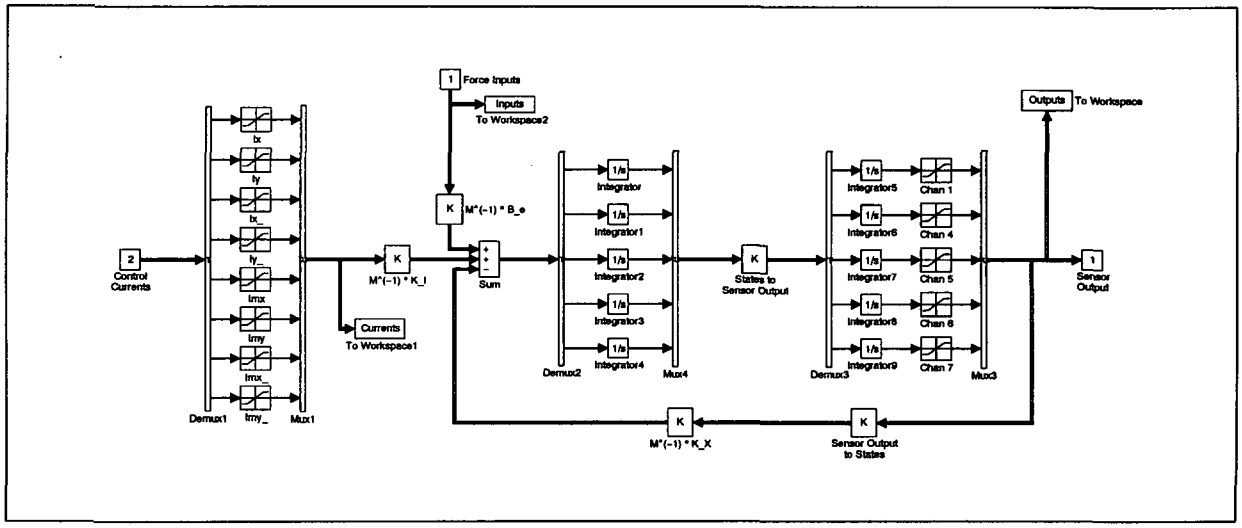

Figure 4: Detail of the *CFVAD III* block as implemented in *Simulink*

the plant is given back to the controller.

The expected disturbance input vector at the laboratory workbench is expected to be composed of both a static loading condition (gravity acting predominantly along the $-z$ axis) and small radial and axial rotor imbalances (which produce both moments about and radial forces along the xy axes for a given spin speed). Consequently, the control actuators are biased at 1.5, 0.0, and 1.0 Amperes for the bias, moment, and radial coils, respectively.

The next section describes the implementation hardware, suspension results, and model validation.

4 Controller Implementation and Results

The control hardware itself is composed of a computer equipped with an Intel 233 MHz *Pentium II* CPU, one 16 channel-16 bit A/D card running in differential mode, and two 12 bit D/A cards. The operating system chosen for this application is a PC Unix clone[4] compliant to the real time *POSIX1b+* standard, and the controller itself is implemented via *C* code that initializes the I/O cards, samples the A/D cards, calculates the control signals, and writes to the D/A cards over a 12.2 kHz throughput. The output from the D/A cards is fed to a set of amplifiers which in turn drive the *CFVAD III* unit. The sensor outputs are filtered via a set of fourth order Chebyshev filters with corner frequencies at 1.0 kHz.

The discretized controller algorithm itself uses the ideal form of the PID controller (6). However, in the controller code – and in order to avoid frequency folding – the PID controllers are warped via the bilinear transformation $s = (2 - \frac{2}{z})/(\tau + \frac{\tau}{z})$ (Oppenheim and Schafer, 1989) where z denotes the so-called Z transform variable, s denotes the Laplace frequency variable, and $\tau = 8.197 \times 10^{-5}$ *seconds* denotes the sampling time. Additionally, a "soft start" method is used, where the controller waits until the rotor has reached its nominal position before activating the integrator terms of (6), thus avoiding integrator windup.

Figure 5 shows the startup behavior of the rotor over the first eight seconds of suspension after the controller is turned on. The first three sub-figures denote the displacement of the center of mass of the impeller along the x, y, and z axes (as defined in Figure 2) as a function of time. The next two sub-figures show the rotation of the rotor about the x and y axes, respectively. In this case, immediately after the controller is turned on, the rotor moves towards its nominal operating point, while acting against the

[4]Linux, kernel 2.0.30

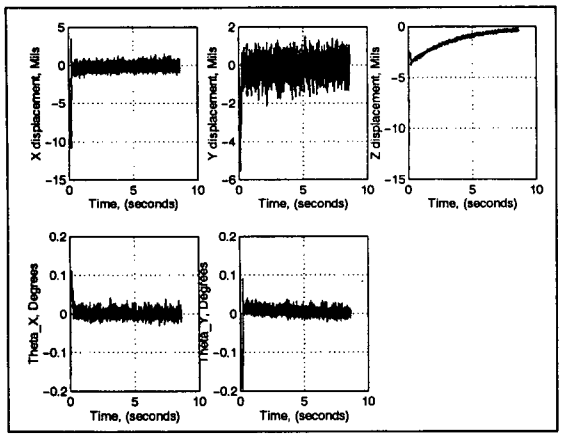

Figure 5: Startup behavior of *CFVAD III* in both x, y, and z displacements, and x and y rotations.

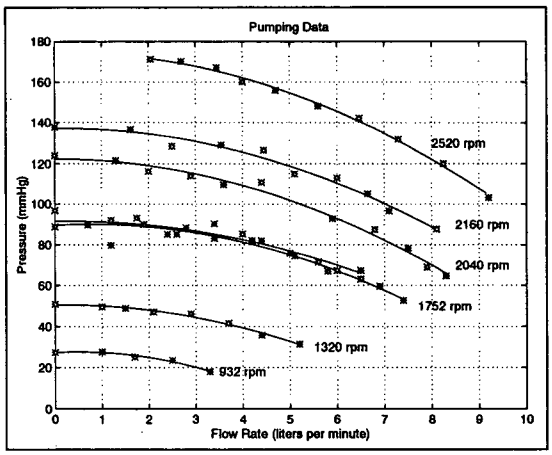

Figure 6: Pumping curves for CFVAD III under varying pressure and flow conditions

gravitational pull acting along the $-z$ axis. This force causes the rotor to sag or maintain a DC offset between itself and the rotor's nominal operating point. This sag, which is most perceptible along the z axis, is reduced once the controller activates the integrators, as dictated by the "soft start" algorithm.

Figure 6 shows the water pumping curves for *CFVAD III* for varying pressures, flows, and rotational speeds of the pump impeller. Note that two sets of data were taken at $1752rpm$ to verify the repeatability of the experiment.

Figure 7 shows a measured frequency response plot obtained by applying a sinusoidal input on the *ith* modal input f_{i_u} and measuring the output along all five of the modal outputs q_j $(\forall j = 1, \ldots, 5)$. In this particular plot, we show only one characteristic curve where the input is applied along the third modal input. Of most importance is the fact that only one modal output (in this case, q_3) is most greatly affected by at least one order of magnitude as compared to all the others. Thus – up to 30 Hz – the model closely resembles the input/output characteristics of *CFVAD III*.

Figure 8 shows the sensor DC and perturbation outputs as a function of tilting the *CFVAD III* housing about the y axis from zero degrees (the rotor's $+z$ axis is parallel to a vector normal to the ground) to 180° (the rotor's $-z$ axis is parallel to a vector normal to the ground). During these experiments, the pump output was maintained at 115 *mmHg* and 6.0 *liters/minute*. As seen from the plots, the rotor did not perceptibly displace from its nominal position. Additionally, the maximum perturbation of the rotor from the nominal changed by no more than 1.5 thousandths of an inch (less than 5% of the total bearing gap). Thus, the controller is able to reasonably control against static external disturbances as well as fluid forces and rotor imbalance.

5 Conclusion

We have shown the plant and the equations of motion for *CFVAD III*. Next, we showed the modally decomposed set of equations and proceeded to introduce a set of five independent PID controllers to said plant. Then, we applied the Routh Hurwitz stability criterion and found four criteria that must be satisfied for each PID controller to stabilize its associated modally decomposed plant. Finally, we showed that we are able to stabilize the plant using said methodology.

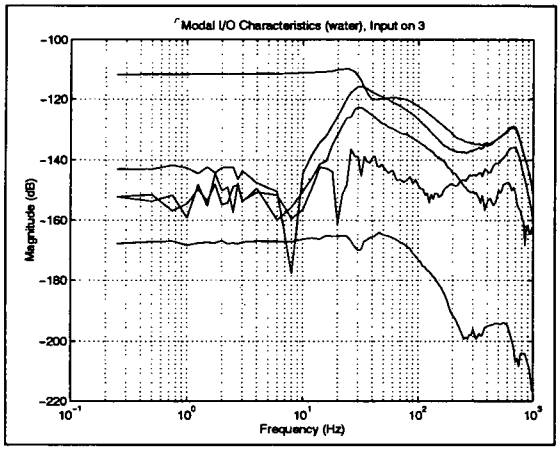

Figure 7: Typical transfer function curve for a given modal input to all five modal outputs. Note that one direction is most heavily influenced than the others (by at least an order of magnitude).

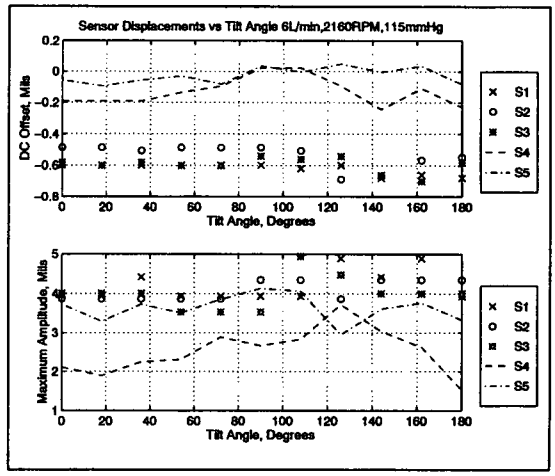

Figure 8: Sensor displacements as a function of housing tilt angle. Here, the pump parameters are 6.0 liters/minute, 115 mmHg, and 2160 RPM

References

P. E. Allaire, H. C. Kim, E. H. Maslen, G. B. Bearnson, and D. B. Olsen. Design of a magnetic bearing supported prototype centrifugal artificial heart pump. In *Tribology Transactions*, volume 39-3, pages 663–669, 1996a.

P. E. Allaire, H.C. Kim, E.H. Maslen, G.B. Bearnson, and D.B. Olsen. Prototype continuous flow ventricular assist device supported on magnetic bearings. In *3rd. Congress of Rotary Flow Blood Pumps*, volume 20, pages 582–590, 1996b.

P. E. Allaire, E. H. Maslen, R. R. Humphris, C. R. Knospe, and D. W. Lewis. Magnetic bearings. In E. R. Boozer, editor, *CRC Handbook of Lubrication and Tribology*, volume 3, pages 577–600, 1994.

M.J. Baloh, P.E. Allaire, E.F. Hilton, N. Wei, J. Decker, E. Maslen, R. Flack, M. Noh, G. Bearnson, and D. Olsen. Design evaluation of magnetic bearing system for a continuous flow blood pump. In *Sixth International Symposium on Magnetic Bearings*, 1998. accepted for publication.

G. B. Bearnson, E. H. Maslen, D. B. Olsen, P. E. Allaire, P. S. Khanwilkar, J. W. Long, and I. C. Kim. Development of a prototype magnetically suspended rotor ventricular assist device. In *Journal of American Society of Artificial Internal Organs*, volume 20-3, pages 275–281, 1996.

Edgar Hilton. Dynamic Model, Controller Design and Implementation, and Analysis for the UVA/Utah Magnetic Suspension Continuous Flow Ventricular Assist Device, *CFVAD III*. Master's thesis, University of Virginia, 1998. (in print).

Katsuhiko Ogata. *Modern Control Engineering*. Prentice Hall, New Jersey, 1990.

A. Oppenheim and R Schafer. *Discrete-Time Signal Processing*. Prentice Hall, 1989.